



## Synthesis and consolidation of $Ti_2SC$ nano layer by spark plasma sintering and its wear behavior

Seyyed Mahdi Hosseini, Akbar Heidarpour\*, Samad Ghasemi

Department of Metallurgy and Materials Engineering, Hamedan University of Technology, Hamedan, Iran.

Received: 23 September 2020; Accepted: 29 October 2020

\* Corresponding author email: [heidarpour@hut.ac.ir](mailto:heidarpour@hut.ac.ir)

### ABSTRACT

In this study, the synthesis of the  $Ti_2SC$  nano layer was investigated by ball milling of Ti,  $FeS_2$ , and C powders. Formation of MAX phase powder after ball milling and after spark plasma sintered (SPSed) sample was characterized by X-ray diffraction (XRD). The morphology and the microstructure of powders were investigated by scanning electron microscopy (SEM) along with energy-dispersive spectroscopy (EDS). The results of the X-ray diffraction patterns showed the reaction between raw materials and the formation of  $Ti_2SC$  and TiC phases as well as  $\alpha$ -Fe, after 10 h ball milling. Iron in the product was removed by an acid washing with 0.5M HCl. Spark plasma sintering at 1450 °C was used to prepare a bulk  $Ti_2SC$  sample. Archimedes' test results showed that the sample was consolidated to 98% of the theoretical density. To evaluate the wear behavior of the bulk sample, a pin-on-disk wear device was used. The results of the wear test showed a low wear rate. This low wear rate was attributed to the self-lubricating nature of the  $Ti_2SC$  nano layer. The friction coefficient for the three forces was also uniform. As the wearing force increased, the wear rate also increased.

**Keywords:** Synthesis,  $Ti_2SC$ , MAX phases, Spark plasma sintering (SPS), Nano layer, wear.

### 1. Introduction

In recent decades, MAX phases, as ternary compounds, have attracted much attention for their unique properties [1]. These materials have a combination of ceramic and metal properties, and therefore sometimes are classified as ductile ceramics. The chemical formula for this class of materials is  $M_{n+1}AX_n$ , where M is a transition metal, A belongs to A group element (often groups 13 and 14), and X is carbon or nitrogen. The value of n is 1, 2, or 3, which according to the value of n, these compounds are divided into three categories of 413, 312, and 211. The crystalline structure of these materials consists of alternating nano layers of M<sub>6</sub>X structures [1,2]

These materials have some metal properties such as good machinability, heat shock resistance, good electrical and thermal conductivity, low hardness, and damage tolerance [3-5]. The MAX phases also have the properties of ceramic materials such as high-temperature resistance, high elastic modulus, and oxidation and corrosion resistance. Therefore, this class of materials has been considered as a new and potential candidate for use in high-temperature applications and severe working conditions [6,7].  $Ti_2SC$  is one of the most important materials in the MAX phase materials with the lowest c/a in its crystal structure. Due to having a low c/a ratio, the mechanical properties of this material are different from other  $M_2AX$  compounds [8]. Du et al. [8]

reported Poisson, shear modulus, and Young's modulus for this material as 0.2, 134, and 322 GPa, respectively. Amini et al. [9] showed that Ti<sub>2</sub>SC hardness is 8 Gpa, which is higher than other MAX phase compositions. Scabarozzi et al. [10] also found that Ti<sub>2</sub>SC had a very high thermal conductivity (~ 60 W/K) at room temperature. The comparison of thermodynamic properties of Ti-S-C and Ti-Al-C systems was performed by Du et al., [11], and also, the structural, tensile, and thermodynamic properties of Ti<sub>2</sub>SC composites were studied by Fu et al. [12]. These remarkable properties make the Ti<sub>2</sub>SC a potential candidate for high-temperature components, heat exchangers, and more.

The Ti<sub>2</sub>SC compound has been synthesized in different ways. Li et al. [13] used the combustion synthesis method; Zhu et al., [14] employed the in-situ synthesis process; Guan et al. [15,16] investigated microwave hybrid heating at low temperature. Also, Chen et al. [17] by heating the titanium, carbon, and iron sulfide; Hosseini et al. [18] by ball milling the titanium, carbon, and iron sulfide; Amini et al. [9] by hot pressing; and Zhou et al. [19] by spark plasma sintering method have synthesized this compound. The mechanism of the SPS process is similar to that of hot pressing (HP), but the mode of production and transfer of heat to the material is different [20]. Spark plasma sintering involves a mechanical loading system under a controlled atmosphere simultaneously with a high-power electrical circuit. In this method, heat is generated by direct current pulses between the particles, and the process of synthesis or sintering is carried out at a lower temperature than the hot press method, and it is possible to achieve high density. In the previous study [18], the Ti<sub>2</sub>SC compound was successfully synthesized by the mechanical milling method. This study aimed to investigate the consolidation of the Ti<sub>2</sub>SC MAX phase by spark plasma sintering. The obtained bulk sample was studied for density, crystalline structure, microstructure, and its wear behavior.

## 2. Materials and methods

In this study, pure commercial titanium, pyrite (FeS<sub>2</sub>), and graphite powders with a purity of higher than 99% and particle size of less than 100 micrometers were used as raw materials. Details of the Ti<sub>2</sub>SC compound synthesis method have been reported in our previous study [18]. For the ball milling process of titanium, pyrite, and graphite powders by the stoichiometry of Ti<sub>2</sub>SC, a planetary

ball mill (Retsch, PM100) at a speed of 500 rpm, and ball to powder ratio of 10 to 1 for 10 hours was used. Phase identification was performed using X-ray diffraction, in the range of 20 to 80°, step size of 0.05°, and a time per step of one second with Cu-Kα radiation (Philips PW-1800 diffractometer). The data obtained from this analysis were evaluated by X'Pert HighScore Plus software. The crystallite size of Ti<sub>2</sub>SC were estimated by analyzing broadening of XRD peaks using Williamson-Hall formula. For morphological and microstructural investigations, the Quanta200 scanning electron microscope, as well as field emission scanning electron microscopy (Czech TESCAN, Mira3) equipped with energy-dispersive spectroscopy was used. The compression of the product resulting from the ball milling process and the preparation of the bulk specimen were carried out using an EF120311 spark plasma sintering equipment. Relative density (apparent density) were calculated by the Archimedes method. The WDRL model of Iran-made pin on the disc was used to evaluate the wear behavior of the bulk specimen. The wear test was performed according to the ASTM G99-04 test method at forces of 100, 500, and 1000 g for a distance of 400 m at a sliding speed of 0.1 m/s.

## 3. Results and discussion

### 3.1. Ti<sub>2</sub>SC powder synthesis

Fig. 1 shows the XRD pattern of the ball-milled specimen after 10 h. As can be seen, the milling product is a Ti<sub>2</sub>SC compound with some TiC. The as-milled powder mixture was annealed at 1000 °C for 2 h, to complete the synthesis of Ti<sub>2</sub>SC. FeS<sub>2</sub> was used as the source of sulfur during synthesis, and as confirmed by the XRD pattern of the 10 h milled pattern, the iron formed during Ti<sub>2</sub>SC synthesis. After ball milling, Ti<sub>2</sub>SC achieved a crystallite size of about 60 nm. Also, for the preparation of the high purity MAX phase, it is necessary to remove iron from the product. For this purpose, the powder was subjected to a half-molar HCl solution for 2 h. XRD pattern of solid powder derived after acid washing is also shown in Fig. 1. As can be seen in Fig. 1, the iron peak is removed from the XRD pattern after acid washing. After annealing at high temperature and the leaching of iron, the crystallite size of the Ti<sub>2</sub>SC MAX phase remain constant. The overall reaction between the raw materials can be considered as equation (1):



It is believed that the synthesis is carried out as a mechanical induced self-sustain reaction (MSR). This type of reaction has also been reported during the milling process for the synthesis of other MAX phase compounds [21-24]. Previous work [18] has elaborated on the mechanism of synthesis and will not be repeated here.

Fig. 2 shows the field scanning electron microscope image of the powder mixture after milling, heat treatment at 1000 °C for 2 hours, and leaching in half-molar HCl solution. As can be seen, the sample is composed of particles with wide size distribution and almost round morphology.

### 3-2 Preparation of bulk sample by spark plasma sintering

The synthesized sample was placed in a graphite mold under 30 MPa pressure at 1450 °C for 10

minutes to prepare the bulk sample by SPS method. The sample was evaluated by the Archimedes test, and the results showed that the relative density was 98%. As can be seen, the high density has been optimally achieved. The diffraction pattern was prepared from the bulk sample and the result is shown in Fig. 3. As can be seen in the diffraction pattern, the sample is composed of  $Ti_2SC$  and  $TiC$  phases. After sintering at 1450 °C, the grain growth of the  $Ti_2SC$  and  $TiC$  phases occurred and the crystallite size of the  $Ti_2SC$  increased to 260 nm.

Fig. 4 shows the FESEM image of the bulk sample. The nano layered structure of the fracture surface of the  $Ti_2SC$  phase is well illustrated in Fig. 4a. As mentioned, the nano layered structure is the main characteristic of the MAX phases [1,2,25], which is well seen in this image. The image from the top of the sample also shows the low porosity

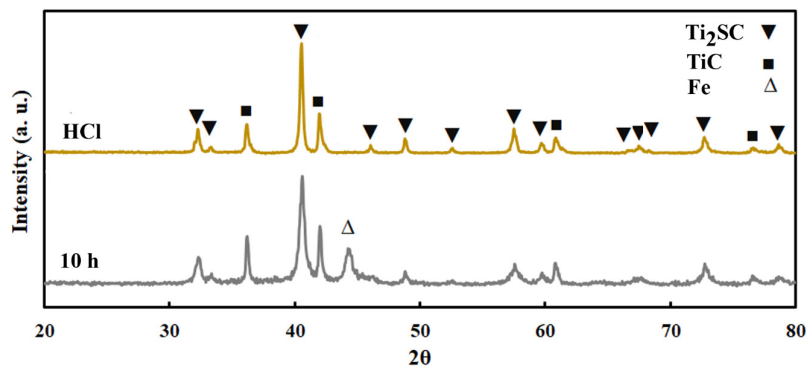


Fig. 1- X-ray diffraction patterns as-received ball milled, after heat treatment, and after leaching.

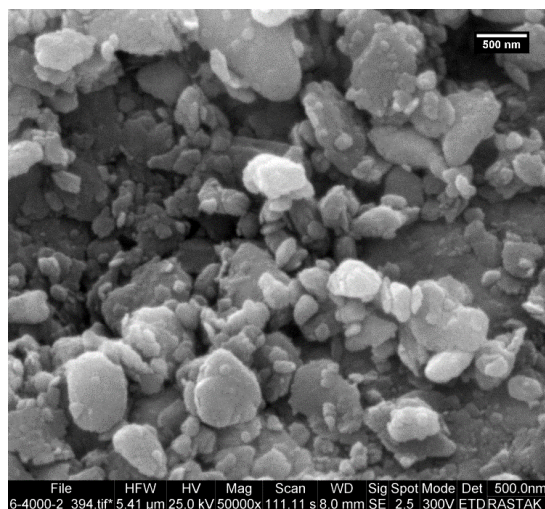


Fig. 2- Scanning electron microscope image of a 10-hour ball milled powder and heat treated at 1000 °C for 2 hours and leached in half-molar HCl solution.

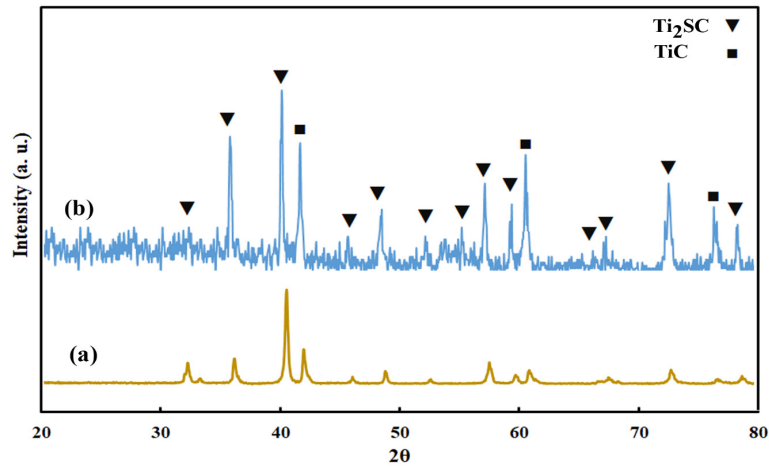


Fig. 3- X-ray diffraction pattern of (a) a 10-hour ball milled powder and heat treated at 1000 °C for 2 hours and leached in half-molar HCl solution, and (b) the sample after spark plasma sintering.

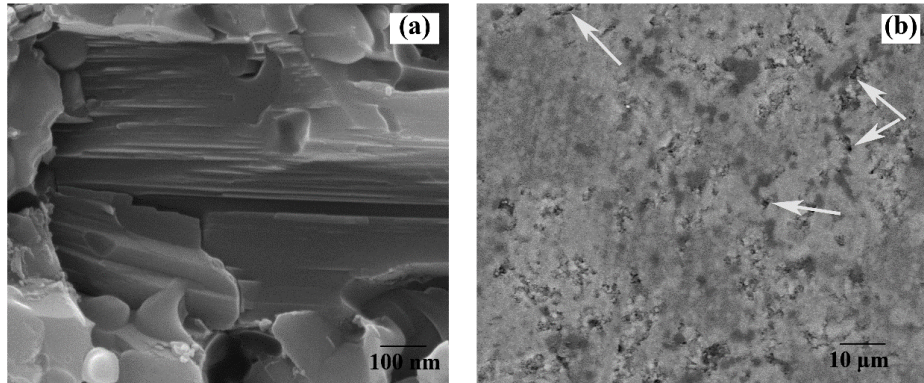


Fig. 4- Scanning electron microscopic image of bulk sample (a) fracture surface, and (b) the top surface.

indicated by the arrows. White areas are  $Ti_2SC$  matrix, and black areas are  $TiC$  particles. The SPS is a sintering process based on the electrical discharge of current pulses between the powder particles and causes a spark. This means that electric current pulses pass between the synthesized powders and when the spark arises from an electrical discharge at the junction or distance between the  $Ti_2SC$  and  $TiC$  powder particles, the local heat generated in the discharge column causes an instantaneous temperature rise, up to 1450 °C. These phenomena cause the particles to bond together. At the microscopic scale, grafting occurs at the contact surface of grains. The sintering of the grains is accomplished by atomic motions on the surface of the powder grains. Fig. 5 schematically illustrates how the current pulse diffuses and passes over  $Ti_2SC$  and  $TiC$  powder particles.

### 3.3 Wear behavior

To study the wear behavior of the  $Ti_2SC$  bulk sample, wear test with 100, 500, and 1000 g forces were performed on the specimen. The wear rate, friction coefficient, and wear surface morphology were investigated and presented in this section. The friction coefficient diagrams are presented in Fig. 6. From this figure, it can be seen that the variation of the friction coefficient is insignificant, and after a few sliding distances, a steady-state condition appears. As shown in Fig. 6, for the applied forces of 100, 500, and 1000 g, the average coefficient of friction was measured 0.2, 0.05, and 0.03, respectively. As shown in Fig. 6, the scattering of data is very small, indicating the nature of the self-lubrication and anti-wear nature of  $Ti_2SC$  nano layer. Actually the nano layered structure of the  $Ti_2SC$  MAX phase cause these phenomena. The

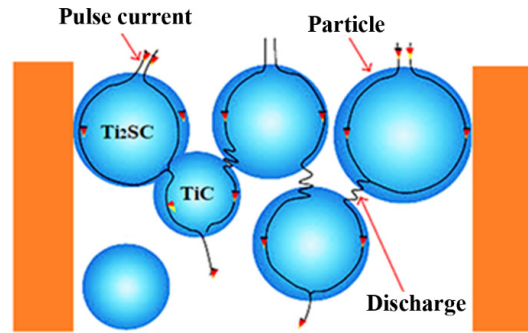


Fig. 5- The schematic representation of the pulses passing through the powder particles and producing heat during the SPS process.

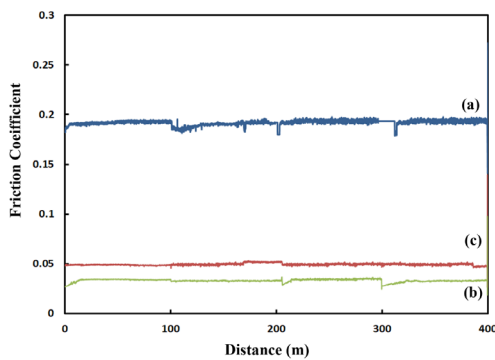


Fig. 6- Friction coefficient diagram in terms of distances under force: (a) 100, (b) 500, and (c) 1000 gr.

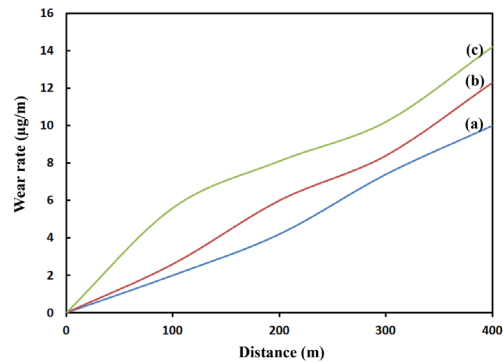


Fig. 7- Wear rate diagram of wearing test under the force of (a) 100, b) 500, and c) 1000 gr..

friction coefficient value decreases as the applied force decreases because of increased mechanical contact between the two surfaces, and enhanced lubricating properties of this material are more pronounced. It should be noted that the crystal structure of the  $Ti_2SC$ , as a MAX phase, is a nano layered structure, and these materials can be considered as solid lubricants. Only at 1000 grams friction force, the data in the friction coefficient graph are scattered, which can be attributed to the separation of particles from the surface and slight change in friction coefficient values. It is also seen at the force of 1000 g at the beginning of the diagram to increase the coefficient of friction and reach a steady-state, which is higher than the diagram for the forces of 100 and 500 g. Also, in all the diagrams in Fig. 6, discontinuities at 100, 200, and 300 m distances relate to the test stop for measurements of mass loss. The measured mass losses were used to calculate the mass change during the wear test.

The wear rate diagrams for the  $Ti_2SC$  bulk sample for the applied forces of 100, 500, and 1000 grams are presented in Fig. 7. The graphs in this figure show that the wear rate increases with

increasing distance as well as with increasing applied force. As can be seen, the wear rates have very low values, indicating that particle deposition and ultra-low mass reduction occurred during the test. The reason for this can be attributed to the self-lubricating property of the  $Ti_2SC$  AMX phase, which makes the wear rate very low. Lu et al., [25] used a combination of  $Ti_2SC$  and CrS to coat the Ti-6Al-4V alloy and showed that the resultant coating is an anti-wear coating, due to the presence of the MAX phase.

The image obtained by scanning electron microscopy of the wear surfaces under different forces is shown in Fig. 8. It should be noted that in this test, no abrasive particles were formed at the contact surface in all three forces. Also, no traces of wear on the steel plate were observed. But at the  $Ti_2SC$  surface, the island regions was observed which were similar to the wear effects. At the contact surfaces, chemical, microstructural, and topographic conditions play an important role, and are altered by several phenomena such as oxidation, phase transformation, amorphization, crystallization, and melting. It can be said that a

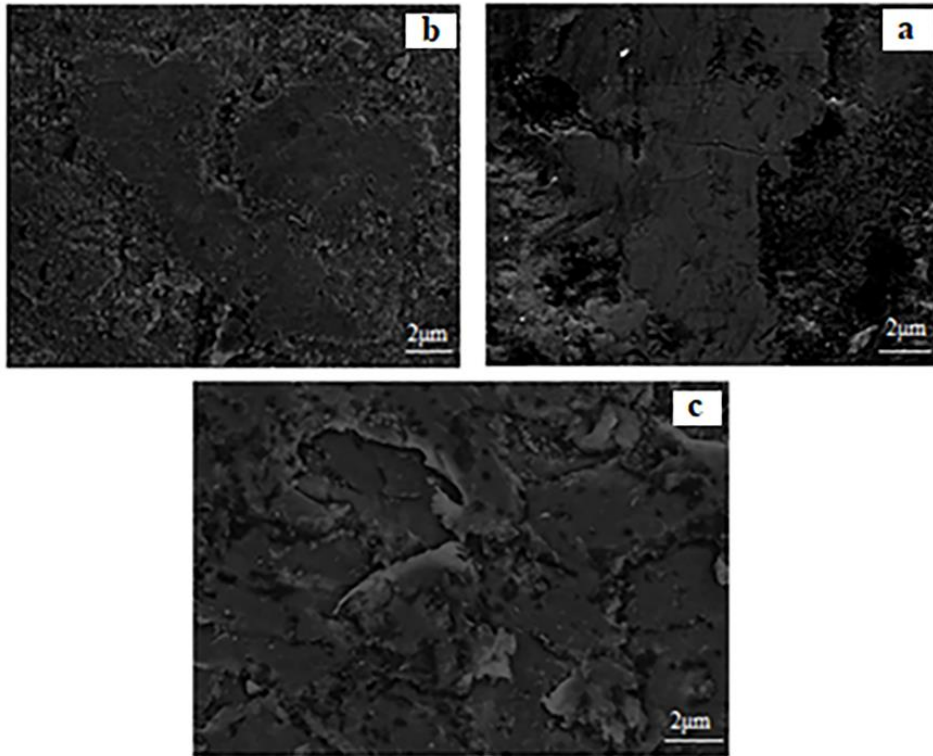


Fig. 8- Field emission scanning electron microscopic image of worn surface under force of (a) 100 gr, b) 500, and c) 1000 gr.

tribo-thin film forms between  $Ti_2SC$  nano layer and the front surface, which is a much-lubricated layer and, as previously mentioned, results in a very low wear rate and smooth friction coefficient. Gupta et al., [26] investigated the wear behavior of  $Ti_2SC$  at ambient and high temperatures. Their results showed that  $Ti_2SC$  is resistant to  $Al_2O_3$  in the ambient temperature range up to 550 °C.

#### 4. Conclusions

- The ternary compound  $Ti_2SC$  nano layer was successfully synthesized after 10 h high-energy ball milling of powder mixture including titanium, graphite and pyrite, and heat treatment at 1000 °C

#### References

1. Rajkumar K, Aravindan S. Microwave sintering of copper-graphite composites. *Journal of Materials Processing Technology*. 2009;209(15-16):5601-5.
2. Koppad PG, Aniruddha Ram HR, Kashyap KT. On shear-lag and thermal mismatch model in multiwalled carbon nanotube/copper matrix nanocomposites. *Journal of Alloys and Compounds*. 2013;549:82-7.
3. Fathy A, Shehata F, Abdelhameed M, Elmahdy M. Compressive and wear resistance of nanometric alumina reinforced copper matrix composites. *Materials & Design* (1980-2015). 2012;36:100-7.
4. Jha P, Gautam RK, Tyagi R, Kumar D. Sliding Wear Behavior

for 2 h with a crystallite size of 60 nm.

- Consolidation by spark plasma sintering under 30 MPa pressure, at 1450 °C for 10 minutes, resulted in the bulk sample of  $Ti_2SC$  with a relative density of 98%. No phase change was observed in the sample after SPS process. The nano layered microstructure was observed for  $Ti_2SC$ , which is a characteristic of MAX phases.

- The results of the wear test showed that with increasing the force, the wear rate increased from 10.1 to 15.1  $\mu g/m$ . This low wear rate was attributed to the self-lubricating nature of  $Ti_2SC$  nano layer compound wear. The friction coefficient for the three forces was also uniform.

- of TiC-Reinforced Cu-4 wt.% Ni Matrix Composites. *Journal of Materials Engineering and Performance*. 2016;25(10):4210-8.
5. Chen Q, Li DY, Cook B. Is porosity always detrimental to the wear resistance of materials?—A computational study on the effect of porosity on erosive wear of TiC/Cu composites. *Wear*. 2009;267(5-8):1153-9.
6. Bagheri GA. The effect of reinforcement percentages on properties of copper matrix composites reinforced with TiC particles. *Journal of Alloys and Compounds*. 2016;676:120-6.
7. Fathy A, Megahed AA. Prediction of abrasive wear rate of in situ Cu- $Al_2O_3$  nanocomposite using artificial neural networks. *The International Journal of Advanced Manufacturing*

- Technology. 2011;62(9-12):953-63.
8. Sharma AS, Mishra N, Biswas K, Basu B. Fretting wear study of Cu–10wt% TiB<sub>2</sub> and Cu–10wt% TiB<sub>2</sub>–10wt% Pb composites. *Wear*. 2013;306(1-2):138-48.
  9. Saravanakumar S, Gopalakrishnan S, Dinaharan I, Kalaiselvan K. Assessment of microstructure and wear behavior of aluminum nitrate reinforced surface composite layers synthesized using friction stir processing on copper substrate. *Surface and Coatings Technology*. 2017;322:51-8.
  10. Chen F, Ying J, Wang Y, Du S, Liu Z, Huang Q. Effects of graphene content on the microstructure and properties of copper matrix composites. *Carbon*. 2016;96:836-42.
  11. Yue H, Yao L, Gao X, Zhang S, Guo E, Zhang H, et al. Effect of ball-milling and graphene contents on the mechanical properties and fracture mechanisms of graphene nanosheets reinforced copper matrix composites. *Journal of Alloys and Compounds*. 2017;691:755-62.
  12. Wang H, Zhang Z-H, Zhang H-M, Hu Z-Y, Li S-L, Cheng X-W. Novel synthesizing and characterization of copper matrix composites reinforced with carbon nanotubes. *Materials Science and Engineering: A*. 2017;696:80-9.
  13. García-Márquez A, Portehault D, Giordano C. Chromium nitride and carbide nanofibers: from composites to mesostructures. *J Mater Chem*. 2011;21(7):2136-43.
  14. Balamurugan P, Uthayakumar M. Influence of Process Parameters on Cu–Fly Ash Composite by Powder Metallurgy Technique. *Materials and Manufacturing Processes*. 2015;30(3):313-9.
  15. Ponraj NV, Azhagurajan A, Vettivel SC, Sahaya Shajan X, Nabhiraj PY, Sivapragash M. Graphene nanosheet as reinforcement agent in copper matrix composite by using powder metallurgy method. *Surfaces and Interfaces*. 2017;6:190-6.
  16. Sheibani S, Ataie A, Heshmati-Manesh S. In-Situ Synthesis of Cu/Cr-Al<sub>2</sub>O<sub>3</sub> Nanocomposite by Mechanical Alloying and Heat Treatment. *Metallurgical and Materials Transactions A*. 2010;41(10):2606-12.
  17. Lu J, Shu S, Qiu F, Wang Y, Jiang Q. Compression properties and abrasive wear behavior of high volume fraction TiC<sub>x</sub>–TiB<sub>2</sub>/Cu composites fabricated by combustion synthesis and hot press consolidation. *Materials & Design*. 2012;40:157-62.
  18. Kingsley JJ, Patil KC. A novel combustion process for the synthesis of fine particle  $\alpha$ -alumina and related oxide materials. *Materials Letters*. 1988;6(11-12):427-32.
  19. Chu A, Guo Z, Ud-din R, Dong Y, Wang L, Liu W, et al. Effect of fuel type on the aminolysis synthesis of CrN powders from combustion synthesis precursors. *Advanced Powder Technology*. 2018;29(6):1439-44.
  20. Chu A, Wang Z, Rafi ud d, Dong Y, Guo C, Liu W, et al. Citric acid-assisted combustion-nitridation-denitridation synthesis of well-distributed W-Cu nanocomposite powders. *International Journal of Refractory Metals and Hard Materials*. 2018;70:232-8.
  21. Frurip DJ, Syverud AN, Chase MW. Thermodynamic properties of diatomic gases at high temperatures: An improved calculational approach for the JANAF thermochemical tables. *Journal of Nuclear Materials*. 1985;130:189-98.
  22. Cao Z, Qin M, Zuo C, Jia B, Liu Y, Gu Y, et al. Effect of glycine on the synthesis of CrN nanopowder using nitridation combustion synthesis precursors. *Journal of Nanoparticle Research*. 2015;17(2).
  23. Nieto A, Bisht A, Lahiri D, Zhang C, Agarwal A. Graphene reinforced metal and ceramic matrix composites: a review. *International Materials Reviews*. 2016;62(5):241-302.
  24. Shi Z, Yan M. The preparation of Al<sub>2</sub>O<sub>3</sub>–Cu composite by internal oxidation. *Applied Surface Science*. 1998;134(1-4):103-6.